

The effects of disc warping on the inclination of planetary orbits

Caroline Terquem

Department of Astrophysics, University of Oxford, Keble Road, Oxford OX1 3RH, UK

Institut d'Astrophysique de Paris, UPMC Univ Paris 06, CNRS, UMR7095, 98 bis bd Arago, F-75014, Paris, France

E-mail: caroline.terquem@astro.ox.ac.uk

ABSTRACT

The interaction between a planet located in the inner region of a disc and the warped outer region is studied. We consider the stage of evolution after the planet has cleared-out a gap, so that the planetary orbit evolves only under the gravitational potential from the disc. We develop a secular analysis and compute the evolution of the orbital elements by solving Lagrange's equations valid to second order in the eccentricity. We also perform numerical simulations with the full disc potential. In general, the interaction between the disc and the planet leads to the precession of the orbit. The orbital plane therefore becomes tilted relative to the disc's inner parts, with no change in the eccentricity. When the inclination approaches 90 degrees, there is an instability and the eccentricity increases. In this case, both the inclination and the eccentricity develop large variations, with the orbit becoming retrograde. As the eccentricity reaches high values, we would expect tidal capture on a short orbit of the planet by the star to occur. This instability happens when the disc is severely warped, or if there is a significant amount of mass in a ring inclined by at least 45 degrees relative to the initial orbital plane. The inclination of the orbit does not depend on the semimajor axis nor on the planet's mass. However, for a significant inclination to be generated on a timescale of at most a few Myr, the planet should be beyond the snow line. The process described here would therefore produce two distinct populations of inclined planets: one with objects beyond the snow line with at most moderate eccentricities, and another with objects on short circularized orbits.

Key words: celestial mechanics — planetary systems — planetary systems: formation — planetary systems: protoplanetary discs — planets and satellites: general

1 INTRODUCTION

As of today, about 250 extrasolar planets have been detected through both radial velocity and transit measurements. The combination of these two detection methods makes it possible to determine the angle between the sky projection of the stellar spin axis and the orbit normal (that we will hereafter call the *projected inclination angle*) using the Rossiter–McLaughlin effect. Among the 70 planets for which this angle has been obtained, about 30 show significant misalignment, with a few even displaying retrograde orbits. The distance of most of these planets to their host star is below 0.1 au, and most of these objects have a mass larger than half that of Jupiter. The sample is therefore highly biased towards massive and close planets. However, these detections indicate that misalignment is not rare.

If planets on short orbits have formed in and migrated through a disc, they would be in a plane misaligned with that of the star’s equator only if the disc itself were misaligned, or if interactions had taken place that would put the planets on misaligned orbits. Such interactions, occurring after dissipation of the disc, include secular perturbation by a distant stellar or planetary companion that produces Kozai cycles with tidal friction (Fabrycky & Tremaine 2007; Wu, Murray & Ramsahai 2007; Naoz et al. 2011), planet–planet scattering (Chatterjee et al. 2008) or secular chaos (Wu & Lithwick 2011). Processes leading to the misalignment of the disc itself include accretion (at later times) of material with angular momentum misaligned with that of the star (Bate, Lodato & Pringle 2010), close encounter with a star while the disc accretes from an extended envelope (Thies et al. 2011), or precession induced by the interaction with a stellar companion in a binary system (Batygin 2012). Planetary orbits inclined with respect to the stellar equatorial plane would also result if the stellar spin axis were tilted due to interaction with the disc (Foucart & Lai 2011; Lai, Foucart & Lin 2011).

The interactions studied so far, which would misalign an orbit initially in the stellar equatorial plane, are presumed to take place after the disc has dissipated. Note, however, that if the orbital plane were inclined relative to the disc while it is still present, the orbit would not necessarily (re)align as a result of the frictional force exerted by the disc on the

planet when it crosses it. This is because the secular gravitational interaction between an inclined planet and the disc's outer parts leads to Kozai cycles that maintain either the inclination or the eccentricity at large values, thus delaying alignment with the disc and circularization of the orbit (Terquem & Ajmia 2010; Teyssandier, Terquem & Papaloizou 2013). This Kozai effect could not be seen in previous simulations of planets on inclined orbits in which the disc was truncated at rather small radii (e.g., Marzari & Nelson 2009), but was observed in the SPH simulations of Xiang-Gruess & Papaloizou (2013) which used a more extended disc and higher orbital inclinations.

So far, the mechanisms that have been put forward to produce a misalignment of a planetary orbit relative to a disc rely on the interaction of the planet with at least one stellar or planetary companion. Here, we investigate the interaction of the planet with the disc itself, and show that a warping of the disc's outer parts may lead to a significant inclination of the planet's orbit relative to the disc's inner parts.

1.1 Warping of protoplanetary discs

The outer parts of protostellar discs may become warped as a result of tidal interaction with a binary star (Terquem & Bertout 1993, 1996; Papaloizou & Terquem 1995). Most stars are in multiple systems (e.g., Köhler 2008) and the distribution of the separation of pre-main sequence binaries has a peak around 30 au (Leinert et al. 1993). It is therefore expected that tidal interactions between a circumstellar disc and the companion are common. If the disc and the orbit are not coplanar, such interactions lead to a warping of the disc's outer parts. Evidence for warped discs have been seen, e.g., in the young triple system WL 20 (Barsony 2002) and in the Bok globule CB 26 (Launhardt & Sargent 2001). Also, in the young binary system HK Tau, the disc around one of the stars is observed not to be coplanar with the orbital plane (Stapelfeldt et al. 1998), which implies that it may be warped.

Warping may also occur if the disc accrete at later times material with angular momentum misaligned with that of the star (Bate, Lodato & Pringle 2010). This is expected as stars form within clusters in which gravitational interactions are important. It was suggested by Tremaine (1991) that the obliquities of the outer planets in our solar system could have been produced by a change in the direction of the angular momentum of the planetary system after it had formed. The proposed causes for this change were a time-dependant angular momentum of the material falling into the disc, possibly due to inhomogeneities

in the collapsing core, or gravitational torques due to mass concentrations within the core. Whether asymmetric infall might actually result in a warped disc or not is still a matter of debate. The accretion of material with misaligned angular momentum onto the disc outer parts does produce an inclination of these outer parts with respect to the inner regions, but such an inclination may be smoothed out by viscous diffusion through the disc. Whether the final configuration is planar or not depends on whether the viscous diffusion timescale is smaller or larger than the precession timescale (see discussion below). In the simulations by Bate, Lodato & Pringle (2010), the disc would settle into a planar configuration for the range of parameters used, but whether it is always the case or not is still an open question.

It has been proposed that, in a stellar binary system in which a disc is misaligned with respect to the orbital plane, planets forming into this disc would themselves be inclined relative to the central star’s equatorial plane (Batygin 2012). This is because the disc is tilted due to the precession of the disc’s angular momentum vector around the orbital angular momentum vector. However, warping was neglected in this study, under the argument that a self-gravitating disc similar to the one considered would only precess as a rigid body if it remained unwarped (see also Batygin et al. 2011).

There have been extensive studies of the dynamics of both galactic and protostellar discs that have shown that, for a disc to precess as a rigid body in a non spherically symmetric potential, it actually has to bend to alter the precession frequency at each radius so that the rate is everywhere the same (Sparke & Casertano 1988; Hofner & Sparke 1994). The disc therefore settles into a discrete bending mode (representing a warp) that is referred to as the modified tilt mode because, in the limit that the external potential is spherically symmetric, it reduces to the trivial rigid-tilt mode. Differential precession can be smoothed out by gravitational torques in a self-gravitating disc (Toomre 1983), and also by radial pressure forces and viscous diffusion (Papaloizou & Terquem 1995, Larwood et al. 1996). These processes are efficient if the timescale on which the different parts of the disc communicate with each other is shorter than the precession timescale. In a protostellar disc in which pressure forces are likely to dominate over self-gravitating forces, rigid body precession is achieved if the sound crossing time through the disc is much smaller than the precession period, so that bending waves propagate through the disc sufficiently fast for the different parts of the disc to adjust their precession rate to a constant value. Communication becomes diffusive in a disc in which turbulent stresses dominate.

In general, in a disc dominated by pressure forces, rigid body precession of the whole

disc is achieved with only a small degree of warping (Larwood et al. 1996, Larwood 1997). In that case, as envisioned by Batygin (2012), the relative inclination of the disc with the central star’s equatorial plane is due mainly to the precession, not to the warp. However, it was found in the numerical simulations of Larwood et al. (1996) that the disc could maintain itself as a long-lived and coherent structure even when a strong warp develops and the inner and outer parts of the disc precess at different rates. In that case, there is a coupling between the two parts of the disc due to pressure gradients, and the rigidly precessing outer parts drag the inner parts behind it.

Planets forming in the disc’s inner parts would therefore interact with the strongly misaligned outer parts, and this is the type of situation we investigate in this paper.

1.2 Setup

We consider a planet that has formed in the inner parts of a disc which outer parts have been warped according, possibly, to one of the processes described in the previous section.

Note that, if the disc’s warp were due to a companion on a noncoplanar orbit in a binary system, gravitational interaction between this companion and the planet would affect the orbital evolution of the planet. This is not taken into account in this paper, where we focus on the interaction between the warped disc and the planet independently of the cause of the warp. The dynamics of a planet in a noncoplanar binary system, taking into account disc warping and the presence of the companion, will be the subject of a further paper.

We consider the stage of evolution after an inner cavity has been opened in the disc, and we assume that the planet’s orbit lies in this cavity. Inner holes are commonly observed in the so-called transitional discs (Andrews et al. 2013). They are usually assumed to be opened either by X-ray photoevaporation (Owen et al. 2011) or by tidal interaction with low mass object(s). A giant planet is expected to clear-out a gap, so that the parts of the disc interior to the orbit are no longer replenished efficiently from the outer disc and accrete onto the central star on a viscous timescale if the disc is active. Note that, in this scenario, the planet may be expected to migrate in as a result of tidal interaction with the outer parts of the disc. However, migration would be slow if the mass of gas in the vicinity of the planet were significantly smaller than the mass of the planet itself. Both planet’s migration and accretion of the disc material would also be very inefficient if the disc were passive in the

region where the planet is located. In that case, the planet would move in a gap but there would still be material interior to its orbit.

In the calculations presented in this paper, we assume for simplicity that there is no mass interior to the planet’s orbit, but our results would hardly be changed if only a gap were cleared, with still material orbiting in the region inside the orbit. This is because the gravitational interaction with the disc is dominated by the parts of the disc which are outside the orbit (Terquem & Ajmia 2010). The important point here is that we assume there is no friction between the disc and the planet, so that the planetary orbit evolves only under the gravitational potential from the disc.

1.3 Plan of the paper

In section 2, we develop a secular analysis of the interaction between a planet and a warped disc. We first write the gravitational potential exerted by the disc on the planet and describe the disc model used in this study in section 2.1. In section 2.2, we expand the potential in the case where the radius of the inner edge of the disc is large compared to the planet’s semimajor axis, and calculate the secular terms as a function of the orbital elements to fourth order in the eccentricity in section 2.3. Lagrange’s planetary equations, valid to second order in the eccentricity, are then written in section 2.4. We solve these equations in section 3, both for a flat and a warped disc, to obtain the evolution of the orbital elements. In the case of a flat disc, we recover the results of Terquem & Ajmia (2010), who showed that perturbation by an outer flat disc inclined relative to the planetary orbit may lead to Kozai cycles. In the case of a warped disc, we find that, in general, the interaction between the planet and the disc leads to the precession of the planetary orbit. The orbit therefore becomes inclined relative to the disc’s inner parts, with no increase of its eccentricity. We find that there is an instability when the inclination approaches 90° . In that case, the eccentricity starts to increase and both the inclination and the eccentricity have very large amplitude variations, with the orbit becoming retrograde. In section 4, we perform simulations that enable us to follow the evolution of the orbit when the eccentricity gets large. Finally, in section 5, we summarize and discuss our results.

2 SECULAR ANALYSIS

2.1 Gravitational potential and disc model

We consider a planet of mass M_p orbiting around a star of mass M_\star which is itself surrounded by a disc of mass M_d . We denote by (x, y, z) a Cartesian coordinate system centred on the star and (r, θ, z) the associated cylindrical polar coordinates. The warped disc has its central parts tangent to the (x, y) -plane and its elevation above this plane is taken to be:

$$z(r, \theta) = \left(\frac{r}{R_o} \right)^p H_o \sin \theta, \quad (1)$$

where R_o is the disc's outer radius, H_o is the maximum elevation at $r = R_o$, and $p > 1$ is an integer which controls the warp's curvature ($p = 1$ would correspond to a disc rigidly tilted relative to the (x, y) -plane). We introduce α , the inclination of the disc's outer edge with respect to the (x, y) -plane, so that:

$$H_o = R_o \tan \alpha, \quad (2)$$

and let R_i be the disc's inner edge. Initially, the orbit of the planet is in the (x, y) -plane and has a semimajor axis $a < R_i$. We suppose that the angular momentum of the disc is large compared to that of the planet's orbit so that the effect of the planet on the disc is negligible.

Note that if the disc as a whole is tilted with respect to the stellar equatorial plane, the (x, y) -plane does not coincide with the equatorial plane of the star. This would be the case if what caused the warp also induced a precession of the disc (e.g., fly-by of a star).

The gravitational potential exerted by the disc at the location of the planet is:

$$\Phi_d = -G \int_{R_i}^{R_o} \Sigma(r) r dr \int_0^{2\pi} \frac{d\theta}{\sqrt{r^2 + r_p^2 - 2rr_p \cos(\theta - \theta_p) + \left[z_p - \left(\frac{r}{R_o} \right)^p R_o \tan \alpha \sin \theta \right]^2}}, \quad (3)$$

where the subscript p refers to the planet, G is the gravitational constant and Σ is the mass density in the disc. We assume:

$$\Sigma(r) = \Sigma_0 \left(\frac{r}{R_o} \right)^{-q}, \quad (4)$$

where q is a positive number. In the numerical simulations described below, we will set $q = 1/2$. The coefficient Σ_0 can be expressed in term of the disc mass M_d :

$$\Sigma_0 = \frac{(-q+2)M_d}{2\pi R_o^2 [1 - (R_i/R_o)^{-q+2}]}. \quad (5)$$

The total potential at the location of the planet has four contributions: one from the disc, which is given by equation (3), one from the central star, an indirect contribution since the center of the coordinate system is accelerated, and another indirect contribution since that, in general, the (x, y) -plane rotates as a result of the disc's precession. However, these last three terms do not yield any secular contribution and will be ignored in this section.

2.2 Expansion of the gravitational potential

We define $u \equiv r_p/r$, $v \equiv z_p/r$ and $m \equiv (r/R_o)^{p-1} \tan \alpha$. The potential in equation (3) can then be written in the form:

$$\Phi_d = -G \int_{R_i}^{R_o} \Sigma(r) dr \mathcal{I}(r, u, v), \quad (6)$$

with:

$$\mathcal{I}(r, u, v) = \int_0^{2\pi} \frac{d\theta}{\sqrt{1 + u^2 - 2u \cos(\theta - \theta_p) + (v - m \sin \theta)^2}}. \quad (7)$$

We assume that $R_i \gg r_p$ and $R_i \gg z_p$ so that u and v are small compared to unity everywhere in the disc. To second-order in u and v , $\mathcal{I}(r, u, v)$ can then be expanded as:

$$\mathcal{I}(r, u, v) = \mathcal{I}(r, 0, 0) + \frac{u^2}{2} \frac{\partial^2 \mathcal{I}}{\partial u^2}(r, 0, 0) + \frac{v^2}{2} \frac{\partial^2 \mathcal{I}}{\partial v^2}(r, 0, 0) + uv \frac{\partial^2 \mathcal{I}}{\partial u \partial v}(r, 0, 0), \quad (8)$$

where the omitted first-order terms vanish. It is shown in the appendix A that this expansion yields the following expression for the potential (6):

$$\Phi_d = -\frac{G\Sigma_0}{R_o} (\mathcal{I}_1 R_o^2 + \mathcal{I}_2 r_p^2 + \mathcal{I}_3 r_p^2 \cos 2\theta_p + \mathcal{I}_4 z_p^2 + \mathcal{I}_5 r_p z_p \sin \theta_p), \quad (9)$$

where $\mathcal{I}_1, \mathcal{I}_2, \mathcal{I}_3, \mathcal{I}_4$ and \mathcal{I}_5 are dimensionless integrals over r which depend only on disc parameters. Their expression in term of elliptic integrals is given in appendix A.

2.3 Secular terms

We wish to calculate the long-term effect of the interaction between the disc and the planet, obtained by averaging the potential (9) over the mean longitude of the planet. In order to perform this averaging, we first express the planet’s polar coordinates r_p, θ_p and z_p in terms of the planet’s orbital elements. We denote by a, e, I, ω and Ω the semimajor axis, eccentricity, inclination, argument of pericentre and longitude of ascending node, respectively, of the orbit, defined with respect to the reference frame (x, y, z) . We then have (Murray & Dermott 1999):

$$r_p \cos \theta_p = R [\cos \Omega \cos (\omega + f) - \sin \Omega \sin (\omega + f) \cos I], \quad (10)$$

$$r_p \sin \theta_p = R [\sin \Omega \cos (\omega + f) + \cos \Omega \sin (\omega + f) \cos I], \quad (11)$$

$$z_p = R \sin (\omega + f) \sin I, \quad (12)$$

where R is the distance between the planet and the star center and f is the true anomaly of the planet (polar angle in the orbital plane relative to the pericentre). To perform a time averaging of the potential (9), we further express $R, \sin f$ and $\cos f$ in terms of the mean anomaly M , which is 2π -periodic and a linear function of time. Expansions of $R, \sin f$ and $\cos f$ to fourth order in e are given in appendix B. We insert these series expansion in equations (10), (11) and (12) above, and expand $r_p^2, r_p^2 \cos 2\theta_p, z_p^2, r_p z_p \sin \theta_p$, and therefore the potential (9), in terms of M to fourth order in e . Finally we perform a time average to obtain the secular potential $\langle \Phi_d \rangle$. Time-averaging eliminates from the expansion the terms which are odd in e . As it happens, the coefficients of e^4 also vanish. The series expansions we obtain are therefore valid up to fifth order in e . The time-averages of $r_p^2, r_p^2 \cos 2\theta_p, z_p^2, r_p z_p \sin \theta_p$, which are needed to compute $\langle \Phi_d \rangle$ from equation (9), are given below:

$$\frac{\langle r_p^2 \rangle}{a^2} = \frac{1}{4} (3 + \cos 2I) + \frac{e^2}{8} [3 (3 + \cos 2I) + 10 \cos 2\omega \sin^2 I] + \mathcal{O}(e^6), \quad (13)$$

$$\begin{aligned} \frac{\langle r_p^2 \cos 2\theta_p \rangle}{a^2} &= \frac{1}{2} \cos 2\Omega \sin^2 I \\ &+ \frac{e^2}{8} [5 (3 + \cos 2I) \cos 2\omega \cos 2\Omega + 6 \cos 2\Omega \sin^2 I - 20 \cos I \sin 2\omega \sin 2\Omega] \\ &+ \mathcal{O}(e^6), \end{aligned} \quad (14)$$

$$\frac{\langle z_p^2 \rangle}{a^2} = \frac{1}{2} \sin^2 I + \frac{e^2}{4} (3 - 5 \cos 2\omega) \sin^2 I + \mathcal{O}(e^6), \quad (15)$$

$$\begin{aligned}
\frac{\langle r_p z_p \sin \theta_p \rangle}{a^2} &= \frac{1}{4} \sin 2I \cos \Omega \\
&+ \frac{e^2}{4} \sin I (3 \cos I \cos \Omega - 5 \cos I \cos 2\omega \cos \Omega + 5 \sin 2\omega \sin \Omega) \\
&+ \mathcal{O}(e^6).
\end{aligned} \tag{16}$$

2.4 Lagrange's planetary equations

In secular theory, the semimajor axis a is constant, and the time variation of e , Ω , ω and I are given by the Lagrange's planetary equations (e.g., Roy 1978):

$$\frac{de}{dt} = -\frac{\sqrt{1-e^2}}{na^2e} \frac{\partial \mathcal{R}}{\partial \omega}, \tag{17}$$

$$\frac{d\Omega}{dt} = \frac{1}{na^2\sqrt{1-e^2}\sin I} \frac{\partial \mathcal{R}}{\partial I}, \tag{18}$$

$$\frac{d\omega}{dt} = \frac{1}{na^2} \left(\frac{\sqrt{1-e^2}}{e} \frac{\partial \mathcal{R}}{\partial e} - \frac{\cot I}{\sqrt{1-e^2}} \frac{\partial \mathcal{R}}{\partial I} \right), \tag{19}$$

$$\frac{dI}{dt} = \frac{1}{na^2\sqrt{1-e^2}} \left(\cot I \frac{\partial \mathcal{R}}{\partial \omega} - \frac{1}{\sin I} \frac{\partial \mathcal{R}}{\partial \Omega} \right), \tag{20}$$

where $\mathcal{R} = -\langle \Phi_d \rangle$ is the disturbing function and $n = \sqrt{G(M_\star + M_p)/a^3}$ is the planet's mean motion. From these equations and the expression (9) of Φ_d , a natural timescale emerges:

$$T = n^{-1} \frac{M_\star + M_p}{\Sigma_0 a^2} \frac{R_o}{a}. \tag{21}$$

Note that, when the evolution of the orbital elements is periodic, in general T is not the period of these oscillations (see section 3). However, equation (21) is important as it gives the scaling of the evolutionary timescale with the different parameters. We see in particular that $T \propto a^{-3/2} M_d^{-1}$.

Having expanded \mathcal{R} to fourth order in e , we obtain $(\partial \mathcal{R}/\partial e)/e$ to second order in e . We insert the time-averaged expressions of r_p^2 , $r_p^2 \cos 2\theta_p$, z_p^2 and $r_p z_p \sin \theta_p$ given by equations (13)–(16) into the potential (9). We then perform the derivatives of $\mathcal{R} = -\langle \Phi_d \rangle$ with respect to e , Ω , ω and I to obtain the dimensionless form of the Lagrangian equations of motion (17)–(20) to second order in e :

$$\begin{aligned}
 T \frac{de}{dt} = e & \left\{ (\mathcal{I}_2 - \mathcal{I}_4) \frac{5}{2} \sin 2\omega \sin^2 I \right. \\
 & + \frac{5\mathcal{I}_3}{4} [(3 + \cos 2I) \sin 2\omega \cos 2\Omega + 4 \cos I \cos 2\omega \sin 2\Omega] \\
 & \left. - \frac{5\mathcal{I}_5}{2} \sin I (\cos I \sin 2\omega \cos \Omega + \cos 2\omega \sin \Omega) \right\}, \quad (22)
 \end{aligned}$$

$$\begin{aligned}
 T \frac{d\Omega}{dt} = & (-\mathcal{I}_2 + \mathcal{I}_4) \frac{\cos I}{2} (2 + 4e^2 - 5e^2 \cos 2\omega) \\
 & + \mathcal{I}_3 \left[\frac{1}{2} \cos I (2 + 4e^2 - 5e^2 \cos 2\omega) \cos 2\Omega + \frac{5}{2} e^2 \sin 2\omega \sin 2\Omega \right] \\
 & + \frac{\mathcal{I}_5}{4 \sin I} [(2 + 4e^2 - 5e^2 \cos 2\omega) \cos 2I \cos \Omega + 5e^2 \cos I \sin 2\omega \sin \Omega], \quad (23)
 \end{aligned}$$

$$\begin{aligned}
 T \frac{d\omega}{dt} = & (\mathcal{I}_2 - \mathcal{I}_4) \frac{1}{8} [5(2 - 3e^2) \cos 2\omega + 10(2 + e^2) \cos 2I \sin^2 \omega] \\
 & + \frac{\mathcal{I}_2}{8} (22 - e^2) + \frac{\mathcal{I}_4}{8} (2 - 11e^2) \\
 & + \mathcal{I}_3 \left\{ \frac{1}{8} \cos 2\Omega [2 - 11e^2 + 5(6 - e^2) \cos 2\omega - 10(2 + e^2) \cos 2I \sin^2 \omega] \right. \\
 & \qquad \qquad \qquad \left. - 5 \cos I \sin 2\omega \sin 2\Omega \right\} \\
 & + \frac{\mathcal{I}_5}{8 \sin I} \left\{ \cos \Omega \cos I [(-2 + e^2)(-3 + 5 \cos 2\omega) - 10(2 + e^2) \cos 2I \sin^2 \omega] \right. \\
 & \qquad \qquad \qquad \left. + 10(1 - e^2 - \cos 2I) \sin 2\omega \sin \Omega \right\} \quad (24)
 \end{aligned}$$

$$\begin{aligned}
 T \frac{dI}{dt} = & (-\mathcal{I}_2 + \mathcal{I}_4) \frac{5}{4} e^2 \sin 2I \sin 2\omega \\
 & + \mathcal{I}_3 \frac{\sin I}{2} [5e^2 \cos I \cos 2\Omega \sin 2\omega + (2 + 4e^2 + 5e^2 \cos 2\omega) \sin 2\Omega] \\
 & + \frac{\mathcal{I}_5}{4} [5e^2 \cos 2I \cos \Omega \sin 2\omega + \cos I (2 + 4e^2 + 5e^2 \cos 2\omega) \sin \Omega] \quad (25)
 \end{aligned}$$

The perturbing function depends on the third Delaunay variable Ω . Thus the Delaunay momentum, which is $\propto \sqrt{1 - e^2} \cos I$, is generally not constant. This is in contrast to the classical Kozai case (e.g., Innanen et al. 1997 and see section 3.1 below).

3 SOLUTION OF THE SECULAR LAGRANGIAN EQUATIONS: ORBITAL EVOLUTION

We solve the set of coupled differential equations (22)–(25) to obtain the evolution of the orbital elements when the planet is subject to the secular gravitational perturbation by the disc. We first focus on the case of a flat disc and then investigate the case of a finite warp.

3.1 Case of a flat disc

The flat disc case is obtained by taking $\tan \alpha = 0$ in equation (2). Therefore, $m = 0$ in equations (A7)–(A10). Since $F_1(0) = F_2(0) = F_3(0) = \pi/2$ and $F_4(0) = 0$, equations (A14)–(A17) give:

$$\mathcal{I}_2 = \frac{\pi}{2} \int_{\rho_i}^1 \frac{\Sigma(\rho)}{\Sigma_0} \rho^{-2} d\rho = \frac{\pi}{2(q+1)} (\rho_i^{-q-1} - 1), \quad (26)$$

$\mathcal{I}_3 = \mathcal{I}_5 = 0$ and $\mathcal{I}_4 = -2\mathcal{I}_2$. In this limit, the potential given by equation (9) reduces to the following expression:

$$\langle \Phi_d \rangle = -\frac{G\Sigma_0}{R_o} \left[\mathcal{I}_1 R_o^2 + 2\mathcal{I}_2 \left(\frac{1}{2} \langle r_p^2 \rangle - \langle z_p^2 \rangle \right) \right], \quad (27)$$

which is of the same form as in the classical Kozai case (Kozai 1962, Lidov 1962), in which an inner body is perturbed by a distant companion on an inclined orbit. When only the secular terms are considered, the Kozai case is equivalent to averaging the mass of the outer companion over its orbit. As pointed out by Terquem & Ajmia (2010), this is analogous to having the inner body perturbed by a disc, as long as most of the disc’s mass is beyond the orbit of the body. We therefore expect that the perturbing potential will have the same form in both cases. Note that here $\langle \Phi_d \rangle$ does not depend on the third Delaunay variable Ω , and therefore $\sqrt{1 - e^2} \cos I$ is constant.

With the above values of the \mathcal{I}_i , the Lagrangian equations of motion (22)–(25) reduce to:

$$T \frac{de}{dt} = \frac{15}{2} \mathcal{I}_2 e \sin 2\omega \sin^2 I, \quad (28)$$

$$T \frac{d\Omega}{dt} = -\frac{3}{2} \mathcal{I}_2 \cos I (2 + 4e^2 - 5e^2 \cos 2\omega), \quad (29)$$

$$T \frac{d\omega}{dt} = \frac{3}{8} \mathcal{I}_2 [6 + 7e^2 + 5(2 - 3e^2) \cos 2\omega + 10(2 + e^2) \cos 2I \sin^2 \omega], \quad (30)$$

$$T \frac{dI}{dt} = -\frac{15}{4} \mathcal{I}_2 e^2 \sin 2\omega \sin 2I. \quad (31)$$

To second order in e , these equations are the same as equations (5) from Innanen et al. (1997), which were derived in the classical Kozai case, provided that we correct an error in their expression for $d\omega/d\tau$, in which the factor $\sqrt{1-e^2}$ should be in the denominator, not in the numerator.

Figure 1 shows e and I versus time, obtained by solving equations (28)–(31) with the following initial values: $e_0 = 10^{-3}$, $\Omega_0 = \omega_0 = 0$ and $I_0 = 55^\circ$. (In this section, we only aim at showing that the equations we use reduce to the classical Kozai case in the appropriate limit, and therefore we do not address the issue of how a planet could start on an inclined orbit.) We have fixed $q = 1/2$ in the expression (4) of Σ , $R_i = 60$ au, $R_o = 80$ au, $M_d = 10^{-2} M_\odot$, $a = 10$ au and $M_p = 10^{-3} M_\odot$. For these parameters, equation (26) gives $\mathcal{I}_2 = 0.565$ and the timescale (21) is $T = 3.8 \times 10^5$ years for $M_\star = 1 M_\odot$. As expected, since I_0 is larger than the critical angle $I_c = \arccos \sqrt{3/5} = 39^\circ.23$, e and I undergo antiphase oscillations (Kozai 1962, Innanen et al. 1997). Note that T is not the period of these oscillations. The inclination angle varies between I_c and I_0 . In theory, as $\sqrt{1-e^2} \cos I$ is constant, the maximum eccentricity should be $\sqrt{1-5 \cos^2 I_0/3} = 0.67$. We see in figure 1 that the maximum eccentricity is actually a bit larger. This is because when e reaches the largest values, the analysis above, which is valid only to second order in e , breaks down and $\sqrt{1-e^2} \cos I$ is not constant (it varies by about 14% in this particular case).

As noted, $p = 1$ in equation (1) corresponds to a disc that is rigidly tilted with respect to the (x, y) -plane. In this case, the term proportional to $\sin \theta$ in the denominator of the integral over θ in the potential (3) can be eliminated by the appropriate choice of coordinates, and this reduces to the Kozai case. Here however, we have defined the orbital elements with respect to the (x, y) -plane and *not* to the plane in which the disc lies when $p = 1$, so we cannot simply recover Kozai’s results when $p = 1$.

3.2 Case of a warped disc

To investigate the warped disc case ($\alpha \neq 0$), we solve equations (22)–(25). Here again we fix $q = 1/2$ in the expression (4) of Σ and we adopt $p = 2$ or 3 in equation (1). In principle, the analysis in this section is valid only for $a \ll R_i$. However, as we will see below, some of the results in this section do not depend on a , and as it happens, any value of $a < R_i$ could be considered.

When the disc reduces to a narrow ring (R_o only slightly larger than R_i), we expect

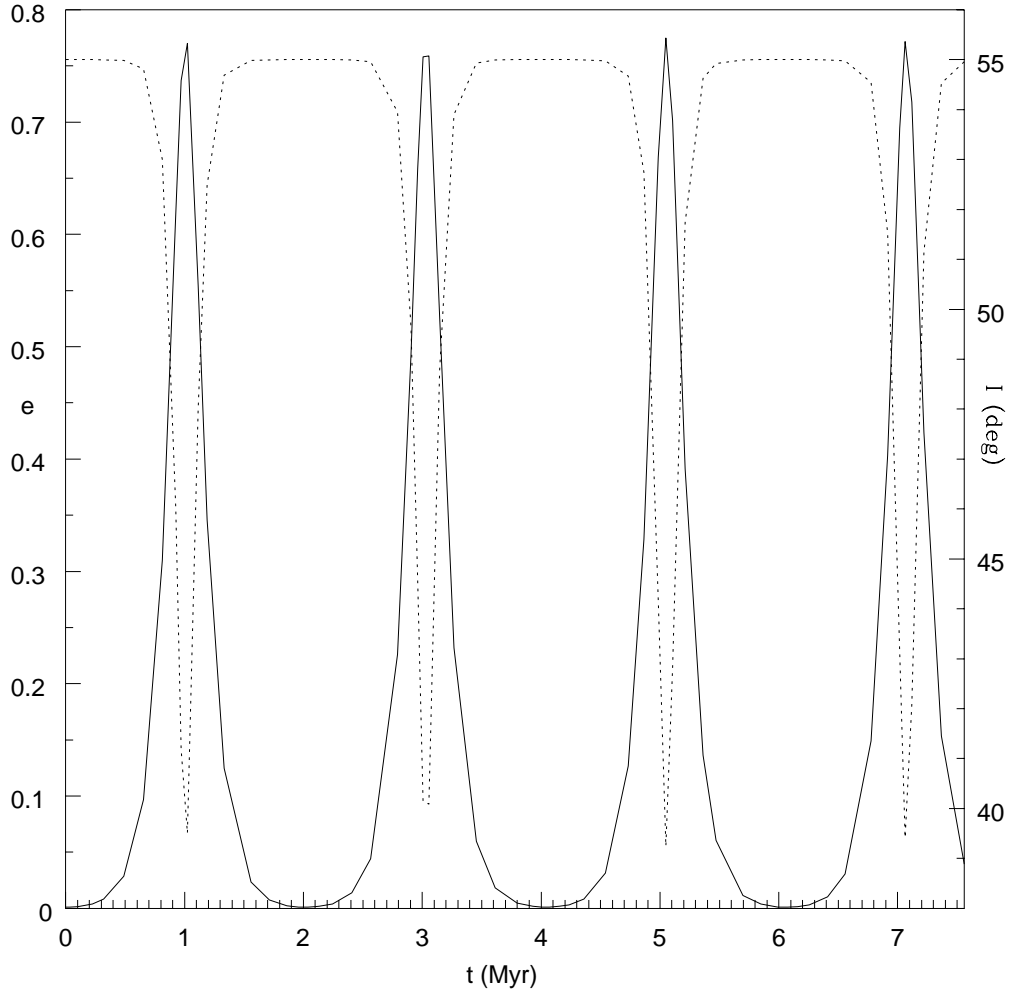


Figure 1. Eccentricity e (solid line) and inclination angle I (in degrees, dotted line) versus time t in Myr for $\alpha = 0$ (flat disc), $a = 10$ au, $M_p = 10^{-3} M_\odot$, $M_d = 10^{-2} M_\odot$, $R_i = 60$ au, $R_o = 80$ au, $e_0 = 10^{-3}$ and $I_0 = 55^\circ$. This illustrates the classical Kozai case, in which e and I undergo antiphase oscillations.

the orbital angular momentum vector \mathbf{L}_{orb} to precess around the total angular momentum vector. Since the ring’s angular momentum is large compared to that of the orbit, this means that \mathbf{L}_{orb} precesses around the ring’s angular momentum vector \mathbf{L}_{ring} . As the ring is inclined by an angle α with respect to the (x, y) -plane, the inclination I of the orbit varies periodically between its initial value I_0 and $I_{\text{max}} = 2\alpha - I_0$ during the precession, independently of a and M_p .

This is illustrated in figure 2, which shows I , ω and Ω versus time for the initial values $e_0 = 10^{-3}$, $I_0 = 10^\circ$ and $\Omega_0 = \omega_0 = 0$, and for $a = 10$ au, $M_p = 10^{-3} M_\odot$, $\alpha = 30^\circ$, $p = 3$, $M_d = 10^{-2} M_\odot$, $R_i = 60$ au and $R_o = 61$ au. We have chosen a finite value of I_0 because, as equations (23) and (24) show, $d\Omega/dt$ and $d\omega/dt$ become infinite when $I \rightarrow 0$. However,

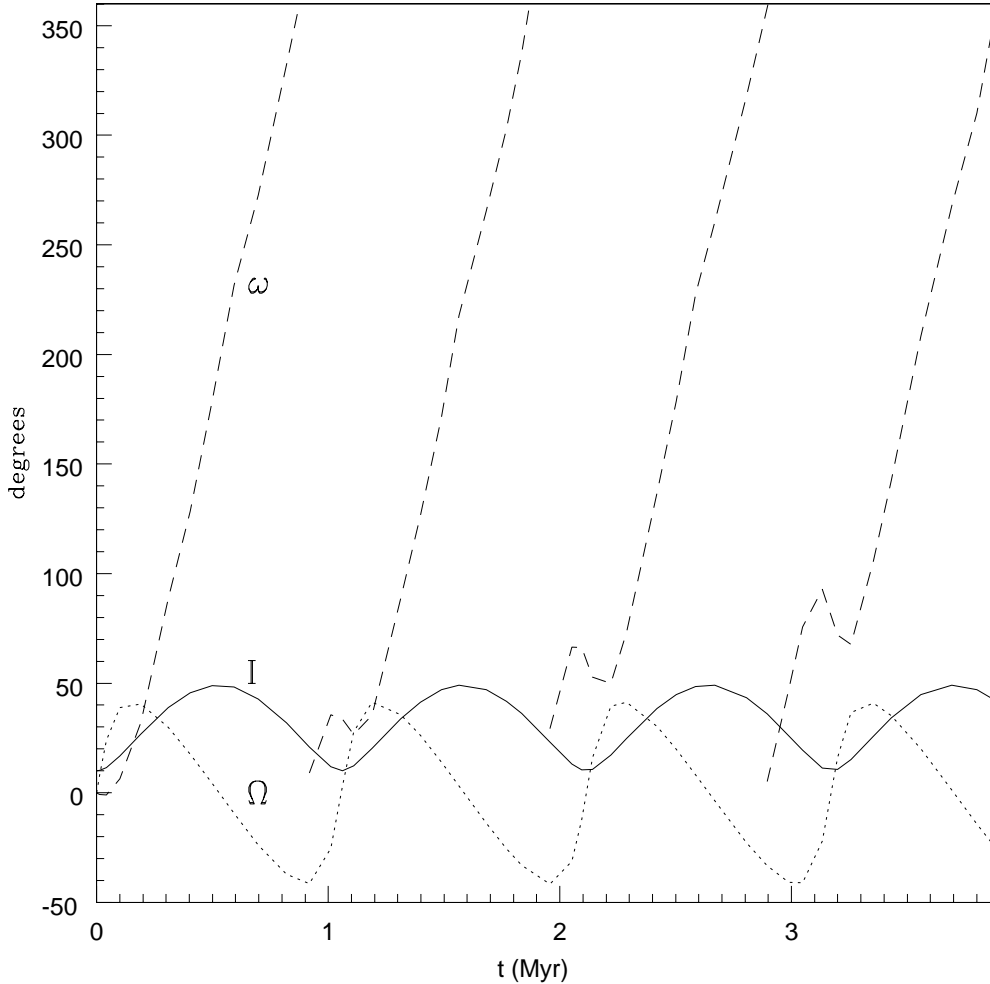


Figure 2. Inclination angle I (solid line), longitude of ascending node Ω (dotted line) and argument of pericentre ω (dashed line) versus time t in Myr for $\alpha = 30^\circ$, $p = 3$, $a = 10$ au, $M_p = 10^{-3} M_\odot$, $M_d = 10^{-2} M_\odot$, $R_i = 60$ au, $R_o = 61$ au, $e_0 = 10^{-3}$ and $I_0 = 10^\circ$. The orbital angular momentum vector precesses around the ring’s angular momentum vector, which causes I to oscillate between 10 and 50° and ω to circulate.

we have checked that exactly the same variations of Ω and I are obtained for $I_0 = 1^\circ$, for example. In this latter case, only the variations of ω are a bit more irregular around the times when I is minimum. As we had anticipated, $I_{\max} = 50^\circ = 2\alpha - I_0$. Also, as expected for a precessing motion, ω circulates uniformly. As can be seen from equation (22), this implies that changes in the eccentricity due to the torque exerted by the disc average to zero over a precession period, so that no secular change of the eccentricity occurs.

Note that exactly the same curves are obtained for different values of a , M_p or M_d . Only the precession period $T_{\text{prec}} \propto a^{-3/2} M_d^{-1}$ changes when these parameters are varied.

In the case displayed in figure 2, the ring is narrow and essentially all of its mass is in a plane inclined by α with respect to the (x, y) -plane. If we now increase the ratio R_o/R_i ,

while keeping M_d fixed, more of the disc's mass will be at smaller inclination with respect to the (x, y) -plane, and therefore the angle between \mathbf{L}_{ring} and \mathbf{L}_{orb} will be smaller. The maximum value reached by I during the precession will accordingly be reduced. For the same parameters as above but with $R_o = 80$ or 100 au, we obtain $I_{\text{max}} = 36^\circ$ or 27° , respectively. If we keep $R_0 = 61$ au but take $R_i = 50$ au, I_{max} is reduced to 40° . These values of I_{max} would be higher for $p = 2$, as in that case the inner parts of the disc would have a higher inclination (see table below).

From equations (1) and (2), we see that the disc can be modelled as a collection of rings of width dr located at a distance r from the central star and inclined with respect to the (x, y) -plane by an angle:

$$\beta(r) = \arctan \left[\left(\frac{r}{R_o} \right)^{p-1} \tan \alpha \right]. \quad (32)$$

The planet will be more affected by rings which are more massive and closer. We therefore define an average inclination angle $\bar{\beta}$ over the whole disc by weighting $\beta(r)$ by the mass of the ring and a function $f(r)$ that decreases with r and such that $f(R_i) = 1$:

$$\bar{\beta} = \frac{1}{M_d} \int_{R_i}^{R_o} 2\pi r dr \Sigma(r) f(r) \beta(r). \quad (33)$$

We would expect the orbital angular momentum vector to precess around the vector inclined by this angle with respect to the vertical axis, and therefore $I_{\text{max}} = 2\bar{\beta} - I_0$. We have found that this is the case to within a good approximation if we take $f(r) = \sqrt{R_i/r}$, which we will adopt thereafter. For the parameters used above, with $R_i = 60$ au and $R_o = 80$ or 100 au, we obtain $\bar{\beta} = 22^\circ$ or 18° , respectively, and therefore $2\bar{\beta} - I_0 = 34^\circ$ or 26° , reasonably close to the values of I_{max} which were found to be 36° and 27° .

Table 1 gives I_{max} and $\bar{\beta}$ for different values of α , R_i and R_o and for $p = 2$ or 3 . In this table, we have considered parameters for which the interaction between the disc and the planet leads to a precession of the orbit. As noted above, I_{max} does not depend on a , and therefore the results listed here are valid for any $a < R_i$, not just $a \ll R_i$. This has been checked by doing numerical simulations using the exact disc potential, i.e. without assuming that a is very small compared to R_i (see section 4).

We use equation (21) to write the precession period T_{prec} as a function of a and M_d and define \bar{T}_{prec} such that:

Table 1. Maximum inclination and precession period in the regime where the orbit precesses for $p = 3$ and $p = 2$.

| α (degrees) | R_i (au) | R_o (au) | p=3 | | | p=2 | | |
|-----------------------|---------------|---------------|----------------------------|-------------------------|----------------------------------|----------------------------|-------------------------|----------------------------------|
| | | | $\bar{\beta}$ (degrees) | I_{\max} (degrees) | \bar{T}_{prec} (Myr) | $\bar{\beta}$ (degrees) | I_{\max} (degrees) | \bar{T}_{prec} (Myr) |
| 30 | 60 | 61 | 29.5 | 59 | 36 | 29.5 | 59 | 36 |
| — | — | 80 | 22 | 45 | 50 | 25 | 52 | 52 |
| — | — | 100 | 18 | 36 | 68 | 21.5 | 46 | 70 |
| — | — | 150 | 12.5 | 23 | 120 | 16.5 | 36 | 124 |
| — | — | 200 | 10 | 16 | 180 | 14 | 30 | 187 |
| 30 | 15 | 100 | 6.5 | 6 | 7.8 | 9.5 | 18 | 8.0 |
| 50 | — | — | 12 | 12 | 8.1 | 17.5 | 35 | 8.6 |
| 70 | — | — | 21 | 24 | 8.8 | 28.5 | 68 | 11 |

The initial conditions are $I_0 = 1^\circ$, $e_0 = 10^{-3}$ and $\Omega_0 = \omega_0 = 0$. I_{\max} is independent of M_d , M_p and a as long as $a < R_i$. The precession period is $T_{\text{prec}} = \bar{T}_{\text{prec}} \times (1 \text{ au}/a)^{3/2} (10 M_J/M_d)$.

$$T_{\text{prec}} = \bar{T}_{\text{prec}} \left(\frac{1 \text{ au}}{a} \right)^{3/2} \frac{10 M_J}{M_d}. \quad (34)$$

\bar{T}_{prec} is given in table 1 for the cases considered and is equal to the precession period for $a = 1 \text{ au}$ and $M_d = 10 M_J$. Note that this precession period is divided by about 10 if we take $a = 5 \text{ au}$. Neither I_{\max} nor T_{prec} depend on M_p . For the initial inclination angle $I_0 = 1^\circ$ used here, we expect $I_{\max} = 2\bar{\beta}$. We note that this is approximately the case, except when R_o/R_i is large and $p = 3$, which corresponds to a disc with very low inclinations in the inner parts.

When I_{\max} gets larger than 90° , the orbit becomes retrograde (more precisely, it would become retrograde relative to the stellar spin if stellar rotation were taken into account). In the case of the narrow ring and for $I_0 = 10^\circ$, this happens for $\alpha > 50^\circ$. For $\alpha = 49^\circ$, $I_{\max} = 88^\circ$ and e stays small (smaller than 3×10^{-3}). In that case, ω still circulates, although not as smoothly as for smaller values of α . For $\alpha = 55^\circ$, $I_{\max} = 100^\circ$ and e grows to 0.23. This is illustrated in figure 3, which shows I , ω , Ω and e for the same parameters as figure 2 except for $\alpha = 55^\circ$. At the beginning of the evolution, ω increases. But as I approaches 90° , ω no longer circulates, so that changes in e no longer average to zero over time and a net increase of the eccentricity is observed.

As α is increased, e becomes too large for the second order analysis of this section to apply.

4 NUMERICAL SIMULATIONS

The analysis presented in the above section is valid only for small values of e . In principle, it is also valid only for $a \ll R_i$. However, as pointed out in the previous section, when the

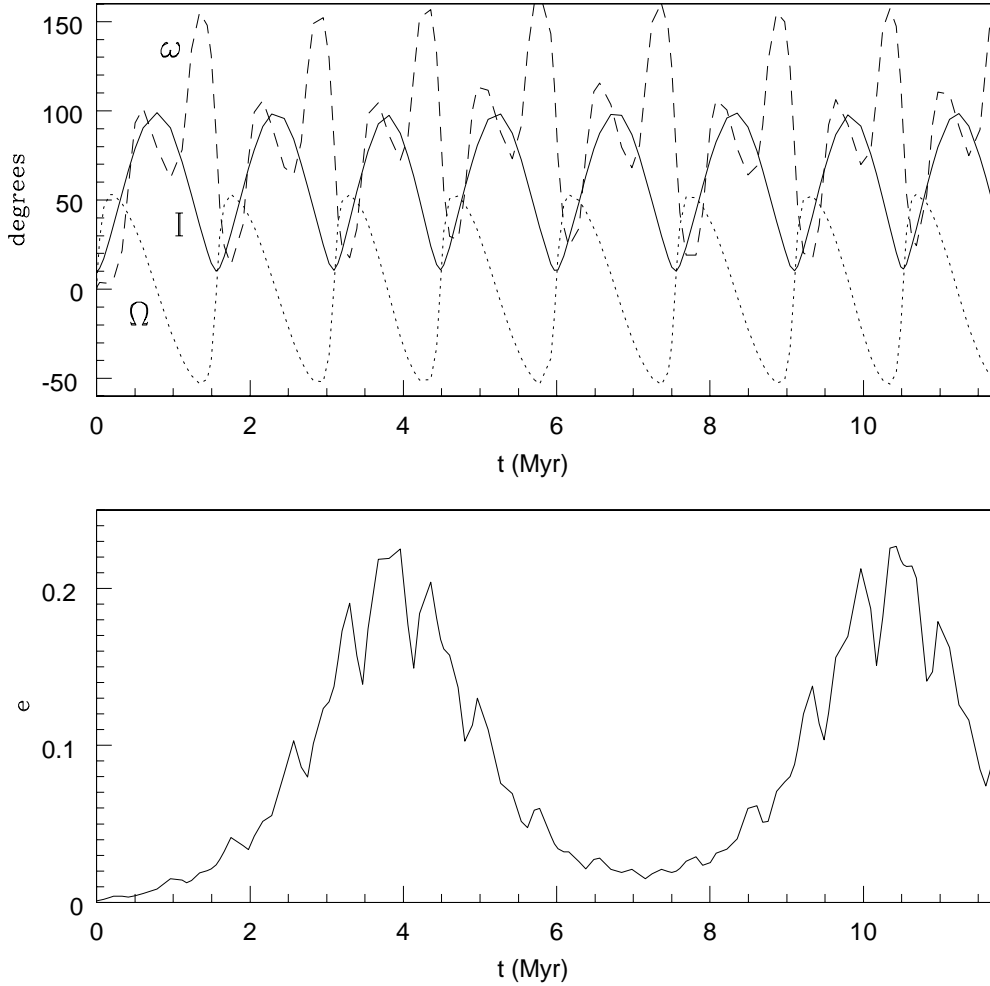


Figure 3. Inclination angle I (solid line, upper plot), longitude of ascending node Ω (dotted line, upper plot), argument of pericentre ω (dashed line, upper plot) and eccentricity e (lower plot) versus time t in Myr for the same parameters as figure 2 except for $\alpha = 55^\circ$. When I approaches 90° , ω no longer circulates and e grows.

planetary orbit precesses, the variations of I do not depend on a and therefore any value of a may be considered in the analysis. To study the evolution of the planet’s orbit in a more general case, we use the N -body code described in Papaloizou & Terquem (2001) in which we have added the gravitational force exerted by the disc onto the planet.

The equation of motion for the planet is:

$$\frac{d^2\mathbf{r}}{dt^2} = -\frac{GM_\star\mathbf{r}}{|\mathbf{r}|^3} - \nabla\Phi_d - \frac{GM_p\mathbf{r}}{|\mathbf{r}|^3} + \mathbf{\Gamma}_{t,r}, \quad (35)$$

where \mathbf{r} is the position vector of the planet and Φ_d is the gravitational potential of the disc given by equation (3). Note that here we use the exact disc potential, so that the results of this section are valid in the general case $a < R_i$, not just $a \ll R_i$. The third term on the right-hand side is the acceleration of the coordinate system based on the central star.

This neglects the net force of the disc on the central star, which would of course require a calculation of the disc response to the planet’s perturbation. Tides raised by the star in the planet and relativistic effects are included through $\mathbf{\Gamma}_{t,r}$, but they are unimportant here as the planet does not approach the star closely. Equation (35) is integrated using the Bulirsch–Stoer method and the integrals involved in $\nabla\Phi_d$ are calculated with the Romberg method (Press et al. 1993).

The planet is set on a circular orbit in the (x, y) –plane at a distance a from the star. As here there is no frictional force acting on the planet, the orbital energy is conserved and the semimajor axis a is constant throughout the evolution of the system. In this paper, we suppose that the planet’s orbit is inside the disc inner cavity ($a < R_i$). If the orbit were still embedded in the disc, the frictional force exerted by the disc on the planet would damp the planet’s inclination and eccentricity, and this would have to be taken into account.

In the simulations reported here, we have taken $q = 1/2$ in the expression (4) of Σ , $p = 3$ in equation (1) and $M_\star = 1 M_\odot$, $M_p = 10^{-3} M_\odot$ and $M_d = 10^{-2} M_\odot$.

Figure (4) shows the evolution of e and I for $\alpha = 70^\circ$, $a = 10$ au, $R_i = 60$ au and $R_o = 80$ au. Note that exactly the same evolution is obtained for different values of M_p . The orbit becomes retrograde and the eccentricity is pumped up to very high values. We have stopped the calculation when, due to the very high eccentricity, the code failed to conserve the energy to within a specified accuracy. As e approaches unity, we expect tidal interaction with the central star to become important and dissipate orbital energy so that e decreases. Ultimately, if the disc does not disappear, the orbit would become circularized on a short orbit. We have verified that we obtain a similar evolution by solving equations (22)–(25) in the early stages when $e \ll 1$.

We observe exactly the same variations of I and e if we take $a = 20$ au instead of $a = 10$ au. The evolution is about three times faster for this wider orbit, which is consistent with an evolutionary timescale proportional to $a^{-3/2}$. Similar behaviour is observed for $p = 2$ (instead of $p = 3$ used here), also on a shorter timescale.

Similar evolution is observed for other values of α . The case displayed in figure 4 is typical, illustrating what happens when the inclination of the orbit passes through 90° : the eccentricity is pumped up to high values and I varies over a broad range of values, including retrograde inclinations.

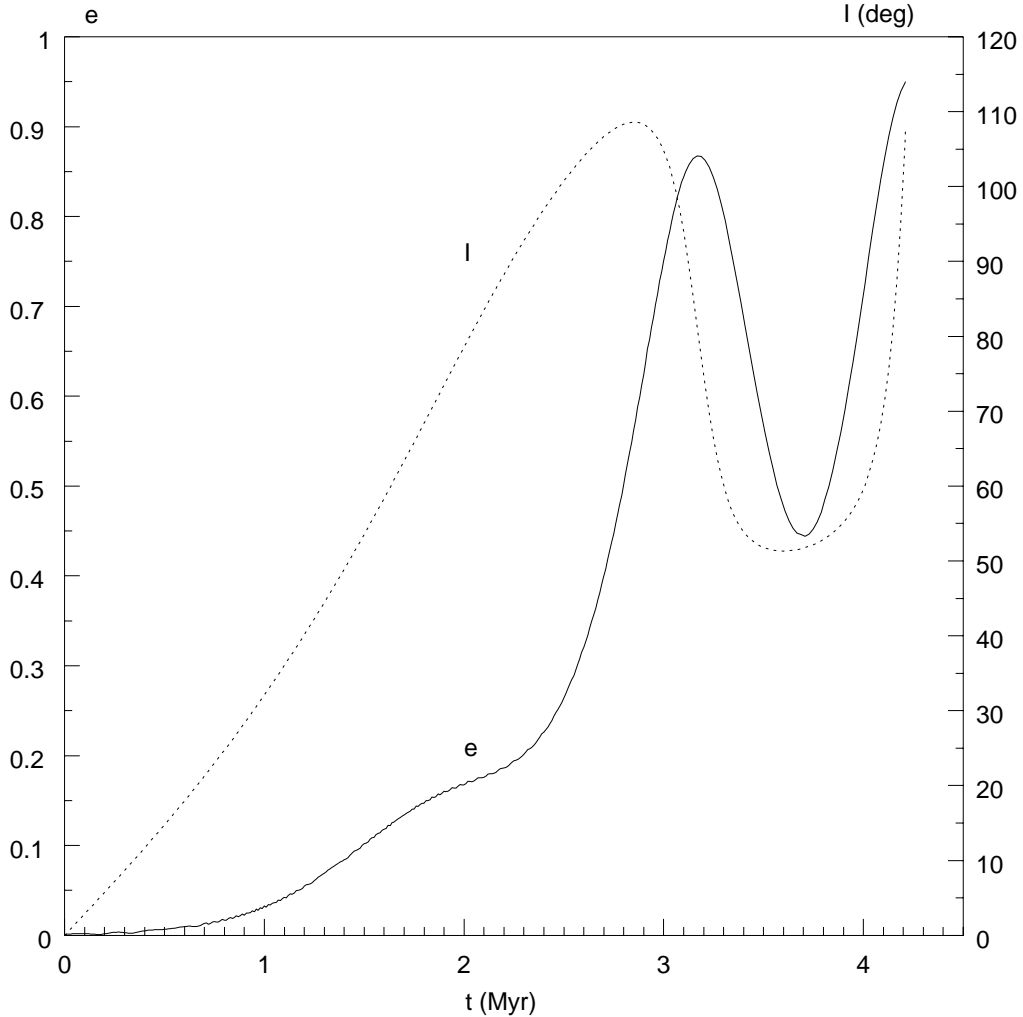


Figure 4. Eccentricity e (solid line) and inclination angle I (in degrees, dotted line) versus time t in Myr for $\alpha = 70^\circ$, $a = 10$ au, $M_p = 10^{-3} M_\odot$, $M_d = 10^{-2} M_\odot$, $R_i = 60$ au and $R_o = 80$ au. The orbit becomes retrograde and the eccentricity is increased to very high values.

5 DISCUSSION

In this paper, we have studied the secular interaction between a planet and a warped disc. We have considered the stage of evolution after the planet has cleared-out a gap. Therefore, there is no friction between the disc and the planet, and the planetary orbit evolves only under the effect of the gravitational potential from the disc. In general, we find that the interaction between the planet and the disc leads to the precession of the orbit. The orbital plane therefore becomes inclined relative to the plane which is tangent to the disc’s inner parts, which we will hereafter call the “reference plane”. If we define some average inclination of the disc with respect to the reference plane, then the inclination of the orbital plane is

twice this averaged angle. The precession of the orbit does not modify its eccentricity: if the planet started on a circular orbit, the eccentricity stays small.

There is an instability when the inclination of the orbital plane relative to the reference plane approaches 90° . The eccentricity of the planet is then built up and both the inclination and the eccentricity develop very large amplitude variations. That happens when the disc is very severely warped, or if there is a significant amount of mass in a ring inclined by a least 45° relative to the initial orbital plane.

Note that the inclination of the orbital plane is measured relative to the disc's inner region. The disc as a whole will in general precess around the central star's equatorial plane, and this will have to be taken into account to compute the inclination of the orbital plane relative to this equatorial plane.

The process studied in this paper shows that the orbit of a planet that has formed in a warped disc could develop a significant inclination when there is no frictional damping.

Although the inclination of the orbital plane does not depend on the planet's semimajor axis a , the timescale for generating a significant inclination does increase as a decreases. For a disc of $\sim 10 M_J$, we typically find that for this timescale to be at most of a few Myr, a has to be larger than 5 au. We therefore expect only planets beyond the snow line to become significantly misaligned through this process. If the warp is such that the orbital plane precesses, the eccentricity is not built up and the planet would be left on its original semimajor axis as the disc dissipates. However, if large eccentricities are generated, the pericentre would become small enough for tidal interaction with the star to circularize the orbit. The planet would then end up on a short orbit, as are the misaligned planets observed so far.

The process described in this paper therefore leads to two distinct populations of misaligned planets: one with objects beyond the snow line and at most moderate eccentricities, and another with objects on short and circular orbits. Of course, the presence of other planets in the system would modify this picture as planet–planet interactions would then change the orbital elements. So far, only planets on short orbits have been detected on inclined orbits. Measurements of the projected inclination angle for more distant objects would help to put constraints on the process discussed here.

ACKNOWLEDGEMENTS

I would like to thank J. Silk for suggesting that the interaction between a planet and a warped disc may drive the inclination of the planetary orbit. It is a pleasure to thank S. Balbus for a critical reading of the manuscript and useful comments.

REFERENCES

- Andrews S. M., Wilner D. J., Espaillat C., Hughes A. M., Dullemond C. P., McClure M. K., Qi C., Brown J. M., 2011, *ApJ*, 732, 42
- Barsony M., Greene T. P., Blake G. A., 2002, *ApJ*, 572, 75
- Bate M. R., Lodato G., Pringle J. E., 2010, *MNRAS*, 401, 1505
- Batygin K., Morbidelli A., Tsiganis K., 2011, *A&A*, 533, 7
- Batygin K., 2012, *Nature*, 491, 418
- Chatterjee S., Ford E. B., Matsumura S., Rasio F. A., 2008, *ApJ*, 686, 580
- Fabrycky D. C., Tremaine S., 2007, *ApJ*, 669, 1298
- Foucart F., Lai D., 2011, *MNRAS*, 412, 2799
- Hofner P., Sparke L. S., 1994, *ApJ*, 428, 466
- Innanen, K. A. and Zheng, J. Q. and Mikkola, S. and Valtonen, M. J., 1997 *AJ*, 113, 1915I
- Köhler R., Neuhauser R., Krämer S., Leinert C., Ott T., Eckart A., 2008, *A&A*, 488, 997
- Kozai Y., 1962, *Astron. J.*, 67, 591
- Lai D., Foucart F., Lin D. N. C., 2011, *MNRAS*, 412, 2790
- Larwood J. D., 1997, *MNRAS*, 290, 490
- Larwood J. D., Nelson R. P., Papaloizou J. C. B., Terquem C., 1996, *MNRAS*, 282, 597
- Launhardt R., Sargent A. I., 2001, *ApJ*, 562, L173
- Leinert C., Zinnecker H., Weitzel N., et al. 1993, *A&A*, 278, 129
- Lidov M. L., 1962, *Planetary Space Science*, 9, 719
- Marzari F., Nelson A. F., 2009, *ApJ*, 705, 1575
- Murray C. D., Dermott S. F., 1999, *Solar System Dynamics*, Cambridge University Press, Cambridge
- Naoz S., Farr W. M., Lithwick Y., Rasio F. A., Teyssandier J., 2011, *Nature*, 473, 187
- Papaloizou J. C. B., Terquem C., 1995, *MNRAS*, 274, 987
- Papaloizou J. C. B., Terquem C., 2001, *MNRAS*, 325, 221
- Press, W. H. and Teukolsky, S. A. and Vetterling, W. T. and Flannery, B. P., 1993, *Numerical recipes in Fortran*, Cambridge Univ. Press
- Roy A. E., 1978, *Orbital motion*, Institute of Physics, London, 4th edition 2005
- Sparke L. S., Casertano S., 1988, *MNRAS*, 234, 873
- Stapelfeldt K. R., Krist J. E., Menard F., Bouvier J., Padgett D. L., Burrows C. J., 1998, *ApJ*, 502, L65
- Terquem C., Ajmia A., 2010, *MNRAS*, 404, 409
- Terquem C., Bertout C., 1993, *A&A*, 274, 291
- Terquem C., Bertout C., *MNRAS*, 279, 415
- Teyssandier J., Terquem C., Papaloizou J. C. B., 2013, *MNRAS*, 428,658
- Thies I., Kroupa P., Goodwin S. P., Stamatellos D., Whitworth A. P., 2011, *MNRAS*, 417, 1817
- Toomre A., 1983, in *IAU Symposium 100, Internal Kinematics and Dynamics of Galaxies*, ed. E. Athanassoula (Dordrecht: Reidel), 177

Tremaine S., 1991, *Icarus*, 89, 85

Wu Y., Murray N. W., Ramsahai J. M., 2007, *ApJ*, 670, 820

Wu Y., Lithwick Y., 2011, *ApJ*, 735, 109

Xiang–Gruess M., Papaloizou J. C. B., 2013, *MNRAS*, 431, 1336

APPENDIX A: EXPRESSION OF THE GRAVITATIONAL POTENTIAL DUE TO THE DISC IN TERMS OF ELLIPTIC INTEGRALS

Using the definition of $\mathcal{I}(r, u, v)$ given by equation (7), we can calculate the different terms that enter its expansion (8):

$$\mathcal{I}(r, 0, 0) = 4F_1(m), \quad (\text{A1})$$

$$\frac{\partial^2 \mathcal{I}}{\partial u^2}(r, 0, 0) = -4F_2(m) + 6F_3(m) + 6 \cos 2\theta_p F_4(m), \quad (\text{A2})$$

$$\frac{\partial^2 \mathcal{I}}{\partial v^2}(r, 0, 0) = -4F_2(m) + 6m^2 [F_3(m) - F_4(m)], \quad (\text{A3})$$

$$\frac{\partial^2 \mathcal{I}}{\partial uv}(r, 0, 0) = 6m \sin \theta_p [F_3(m) - F_4(m)], \quad (\text{A4})$$

where we have defined, for $i = 1, 2$ or 3 :

$$F_i(m) = \int_0^{\pi/2} \frac{d\theta}{(1 + m^2 \sin^2 \theta)^{(2i-1)/2}}, \quad (\text{A5})$$

and:

$$F_4(m) = \int_0^{\pi/2} \frac{\cos 2\theta d\theta}{(1 + m^2 \sin^2 \theta)^{5/2}}. \quad (\text{A6})$$

We recall that $m = (r/R_o)^{p-1} \tan \alpha$. The F_i can be expressed in terms of the complete elliptic integrals of the first and second kind, K and E respectively:

$$F_1(m) = \frac{1}{\sqrt{1+m^2}} K \left(\frac{m^2}{1+m^2} \right), \quad (\text{A7})$$

$$F_2(m) = \frac{1}{\sqrt{1+m^2}} E \left(\frac{m^2}{1+m^2} \right), \quad (\text{A8})$$

$$F_3(m) = \frac{1}{3(1+m^2)^{3/2}} \left[2(2+m^2) E\left(\frac{m^2}{1+m^2}\right) - K\left(\frac{m^2}{1+m^2}\right) \right], \quad (\text{A9})$$

$$F_4(m) = \frac{1}{3m^2(1+m^2)^{3/2}} \left[2(1+m^2+m^4) E\left(\frac{m^2}{1+m^2}\right) - (2+m^2) K\left(\frac{m^2}{1+m^2}\right) \right], \quad (\text{A10})$$

where K and E are defined as:

$$K(u) = \int_0^{\pi/2} \frac{d\theta}{\sqrt{1-u\sin^2\theta}}, \quad (\text{A11})$$

$$E(u) = \int_0^{\pi/2} \sqrt{1-u\sin^2\theta} d\theta, \quad (\text{A12})$$

with $u < 1$. Note that $F_4(0)$ should be calculated using equation (A6) instead of equation (A10).

By inserting the expansion of \mathcal{I} given by equation (8) into the expression of the potential Φ_d given by equation (6), we then get the potential under the form given by equation (9) with:

$$\mathcal{I}_1 = \int_{\rho_i}^1 4\bar{\Sigma}(\rho) F_1(m) d\rho, \quad (\text{A13})$$

$$\mathcal{I}_2 = \int_{\rho_i}^1 \bar{\Sigma}(\rho) \rho^{-2} [-2F_2(m) + 3F_3(m)] d\rho, \quad (\text{A14})$$

$$\mathcal{I}_3 = \int_{\rho_i}^1 3\bar{\Sigma}(\rho) \rho^{-2} F_4(m) d\rho, \quad (\text{A15})$$

$$\mathcal{I}_4 = \int_{\rho_i}^1 \bar{\Sigma}(\rho) \rho^{-2} \{-2F_2(m) + 3m^2 [F_3(m) - F_4(m)]\} d\rho, \quad (\text{A16})$$

$$\mathcal{I}_5 = \int_{\rho_i}^1 6m\rho^{-2} \bar{\Sigma}(\rho) [F_3(m) - F_4(m)] d\rho \quad (\text{A17})$$

with $\rho = r/R_o$, $\rho_i = R_i/R_o$ and $\bar{\Sigma}(\rho) = \Sigma(\rho)/\Sigma_0$. Note that $m = \rho^{p-1} \tan \alpha$.

APPENDIX B: SERIES EXPANSION OF R , $\sin F$ AND $\cos F$ IN TERMS OF THE MEAN ANOMALY TO FOURTH ORDER IN THE ECCENTRICITY

The series expansions of R , $\sin f$ and $\cos f$ in terms of M to fourth order in e are given, e.g., in Murray & Dermott (1999), and we recall them below:

$$\begin{aligned} \frac{R}{a} = 1 - e \cos M + \frac{e^2}{2} (1 - \cos 2M) &+ \frac{3e^3}{8} (\cos M - \cos 3M) \\ &+ \frac{e^4}{3} (\cos 2M - \cos 4M) + \mathcal{O}(e^5), \end{aligned} \quad (\text{B1})$$

$$\begin{aligned} \sin f = \sin M &+ e \sin 2M + \frac{e^2}{8} (9 \sin 3M - 7 \sin M) + \frac{e^3}{3} \left(4 \sin 4M - \frac{7}{2} \sin 2M \right) \\ &+ \frac{e^4}{64} \left(\frac{17}{3} \sin M - \frac{207}{2} \sin 3M + \frac{625}{6} \sin 5M \right) + \mathcal{O}(e^5), \end{aligned} \quad (\text{B2})$$

$$\begin{aligned} \cos f = \cos M &+ e (\cos 2M - 1) + \frac{9e^2}{8} (\cos 3M - \cos M) + \frac{4e^3}{3} (\cos 4M - \cos 2M) \\ &+ \frac{25e^4}{64} \left(\frac{1}{3} \cos M - \frac{9}{2} \cos 3M + \frac{25}{6} \cos 5M \right) + \mathcal{O}(e^5). \end{aligned} \quad (\text{B3})$$